Pore-scale oxygen (O_2) dynamics of vadose zone under dry-wet cycles of artificial recharge: A soil lysimeter experiment

Tanushree Dutta[a,*], Albert Carles-Brangarí[a], Daniel Fernàndez-Garcia[a], SimonettaRubol[a,b], Joel Tirado-Conde[a], Xavier Sanchez-Vila[a]

[a]*Hydrogeology Group, Department of Geotechnical Engineering and Geosciences, Universitat Politècnica de Catalunya - BarcelonaTech, Spain*

[b]*Department of Mechanic, Civil and Environmental Engineering, University of Trento, Italy*

[*]Corresponding author: *tanushree.dutta@upc.edu* *(T.Dutta)*

ABSTRACT

Vadose zone oxygen dynamics control all subsurface redox reactions and play a decisive role in maintaining groundwater quality. Although drying and wetting events are common in artificial recharge, their effects on subsurface oxygen distribution are poorly documented. We monitored oxygen concentration in the unsaturated zone in a mid-scale (1 m high) laboratory soil lysimeter, which was subjected to short wetting and drying cycles that simulated a highly permeable shallow aquifer recharged by river water. Ten cycles of varying duration were performed for a period of 85 days. Measurements of oxygen in the liquid and the gas phases were recorded every 20 seconds using non-invasive optical fibers (PreSens). The results provided high-resolution (in time) oxygen concentration maps. The infiltration rate revealed a decreasing trend during wetting cycles associated with biological clogging. Such a decrease with time was accompanied by a depletion of O_2 concentration, occurring within the first few hours of the

Article publicat[1] / ***Published paper*:**

Dutta, Tanushree; Carles Brangari, Albert; Fernández García, Daniel; Rubol, Simonetta; Sánchez Vila, Francisco Javier; Tirado Conde, Joel (2014) Vadose zone oxygen (O_2) dynamics during drying and wetting cycles: An artificial recharge laboratory experiment. Journal of Hydrology, 527, 10.1016/j.jhydrol.2015.04.048

---

infiltration. During drying, O_2 concentrations recovered rapidly at all depths owing to air flushing, resulting in a stratified vertical profile consistent with the biological consumption of O_2 along the air infiltration path. Furthermore, drying periods caused a potential recovery of the infiltration capacity while preserving the soil biological activity. Scraping also led to the recovery of the infiltration capacity of the soil but was less effective than drying. Our experiment suggests that the small-scale heterogeneity played a key role in accurately mapping pore-scale O_2 concentrations and should be considered in modeling O_2 fluxes of unsaturated soils under natural or managed recharge conditions.

Keywords: Oxygen concentration dynamics, precision sensing, Managed Aquifer Recharge, infiltration, drying-wetting cycles, biological processes

HIGHLIGHTS

- Successive wet-dry cycles of artificial recharge alter the infiltration rates with time
- Oxygen concentration stabilizes within few hours of commencement of infiltration and drying
- Drying restores the infiltration rate close to its initial value
- Surface scraping results in an immediate but temporary increase in the infiltration rate
- Quantifying small changes in space and time is vital for accurate pore-scale O_2 mapping

1. Introduction

Subsurface redox zonation is driven by the spatial and temporal distribution of oxygen that serves as the primary terminal electron acceptor during the degradation of organic carbon (Greskowiak et al., 2006). Understanding oxygen zonation in artificial recharge is important for two reasons: (a) biodegradation of hydrocarbons demands aerobic conditions (Rifai et al., 1995; Christensen et al., 2000), and (b) biodegradation of halogenated compounds requires reducing conditions (Bouwer, 1994; McCarthy and Semprini, 1994; Vogel, 1994). Moreover, bio-denitrification takes place preferentially under anaerobic conditions (Schmidt et al., 2011; Rubol et al., 2012). Thus, in order to better understand organic and inorganic contaminants in aquifer systems, it is necessary to carry out a detailed mapping of the subsurface distribution of oxygen and to elucidate the transport processes. Artificial recharge of groundwater from available surface water is an important management strategy for replenishing groundwater supplies while improving water quality (Dillon, 2005; Fox et al., 2006). The extent to which conditions in these managed systems can be optimized to achieve an adequate water supply (involving both quantity and quality aspects) depends largely upon the physical, geochemical and biological processes that occur in the vadose zone.

Application of surface water or wastewater in rapid infiltration systems is cyclic and typically consists of a period of water application (flooding) followed by days or weeks of drying (Bouwer and Rice, 1984; NRMRI, 2006; US EPA, 1984). Drying is often accompanied by scraping the low-permeability layer on the pond’s floor (e.g., Mousavi and Rezai, 1999). This is a way to recover aerobic conditions of the topsoil surface and the infiltration capacity, and to renew the soil´s capability of biodegradation (e.g., Bouwer, 2002). The hydraulic loading rate within each wetting cycle affects oxygen availability, pore-fluid velocity and retention time. However, it is not possible to assess the optimal ratios of flooding/drying periods owing to the complexity and difficulty in accurately measuring and mapping the spatial and temporal distribution of oxygen concentrations in the field (Akhavan et al.,2013).

Soil pore oxygen concentration depends on the interaction between transport and consumption processes. The former is regulated by advection and diffusion, whereas the latter occurs via chemical reactions and microbial activity. Hot-moments, which are defined by McClain et al. (2003) as short periods that display very high reaction rates with respect to longer intervening periods, affect microbial activity directly (Schimel et al., 2007) or indirectly by changing the redox conditions and O_2 availability (e.g., Rubol et al., 2012). High resolution O_2 maps of soil metabolic activity revealed the presence of these hot-moments in riverbed sediments (Dutta and Rubol, 2014). Microbes can adapt to fluctuations of redox conditions by changing their function or composition (DeAngelis et al., 2010), or protecting themselves by forming biofilms (Romaní et al., 2004). Biofilm formation may result in biological clogging, which could reduce the hydraulic conductivity of the soil by several orders of magnitude (Baveye et al., 1998; Bouwer and Rice, 2001) and alter the soil's water retention capacity (Rubol et al., 2014). Infiltration rates may also be affected by temperature, either directly due to the dependence of water viscosity on temperature (Constantz, 1982; Jaynes, 1990), or indirectly as temperature affects biological activity (Le Bihan and Lessard, 2000). Notwithstanding, a poor knowledge of the pore-scale processes and the lack of instrumentation techniques to capture small-scale heterogeneity prevents us from proper upscaling from micro to larger macro scale (Krause et al., 2014).

In the present study, using a 1m high lysimeter equipped with an array of sensors, we monitored a number of physical and chemical parameters continuously over a period of 85 days in order to link the spatial and temporal dynamics of fluid flow, water retention, and pore-scale O_2

concentration distribution with depth and time during the succession of wetting and drying cycles. The experimental setup also allowed us to assess the changes in the infiltration capacity resulting from the drying phases.

2. Materials and Methods

2.1. Soil Collection, Preparation and Characterization

Soil was collected from the prodelta region of the Llobregat River in a Managed Aquifer Recharge facility located in Sant Vicenç dels Horts, Spain (418446.63 N, 4581658.18 E, zone 31T). Pebbles and coarse grains were removed by passing the soil through a sieve of 0.2 cm. As a result, the amount of fine grains increased, facilitating permeability and the soil's capacity to generate bacterial activity. By using a sieve of 0.2 cm, the architecture of soil aggregates was preserved.

Representative soil samples were analyzed for particle size distribution, pH and dissolved organic carbon (DOC, organic carbon analyzer model Shimadzu TOC-V-CSH 230V). A small composite sample was extracted using 2M KCl for the determination of ammonium and nitrate. The extractants were analyzed using an Ionic chromatograph (model-DIONEX IC5000) equipped with an autosampler with an eluant flow rate 1 mL/min, an IonPac® AS18 anion-exchange column (4x250mm) with an AG Guard column (4x50 mm) and an IonPac® CS16 cation-exchange column (5x250mm) with a CG Guard column (5x50 mm).

Analysis of particle size distribution (ASTM, 2000) indicated that the soils were largely composed of medium sand (>80%, see Table 3). X-ray powder diffraction analysis of a sample of soil located nearby revealed that the soil consisted mostly of quartz, with an observable amount of calcite and traces of dolomite, albite, clinochore, muscovite and orthoclase (exact proportions not known). Chemical characteristics of the sediment are listed in Table 3.

2.2. Lysimeter Set-up, Packing and Chemical sink addition

A rectangular shaped lysimeter was constructed following the method described in Rubol et al. (2014) (see Fig 1 for the complete setup). The lysimeter was made of plexiglass, and was 1.2 m high, 0.46 m long, and 0.15 m wide to minimize boundary effects and to allow for some degree of heterogeneity in both the vertical and horizontal directions. All the instrumentation and materials (except the soil) were autoclaved.

The lower 15 cm of the tank was filled with silica sand (0.7 to 1.8 mm diameter, supplied by Triturados Barcelona, Inc.) and was covered with a geo-synthetic membrane to prevent flushing of the smaller particles out of the system. The upper 85 cm of the tank was filled with the sieved soil to minimize perturbations both in soil conditions and existing cellular biodiversity. Granular materials were placed layer by layer (10 cm thick) and were packed manually to attain an adequate consistency. Additional compaction occurred owing to the hydrostatic forces created by successive filling and emptying of the device but no additional shrinkage was observed. Filling took place from the bottom to avoid bubble retention. Porosity values were determined from the saturated water content, ranging from 0.27 to 0.38 depending on the sensor location. An initial dry bulk density of 1.38 g/cm^3 was measured.

The top 20 cm of the tank was left empty to allow ponding and infiltration conditions to develop during wetting periods. The height of the water above the soil surface was maintained at a fairly constant level by means of a regulated peristaltic pumping system. Using this device, the system was fed with chemically controlled (synthetic) water with no recirculation. The synthetic water was made up of the chemical signature compounds of the river Llobregat (see Table 1). Organic and inorganic compounds (see Table 1 for compositions) were mixed with deionized water daily in order to minimize variations in its chemical composition with time. To monitor the infiltration rate, pumped water and water level at the pond were recorded. Infiltration as a function of time was estimated by applying water balance considerations at the pond. The rate of evaporation during the wetting phases was negligible compared with the infiltration rate. During drying periods, the water feeding system was substituted by an array of five 15W light bulbs. These bulbs were placed 15cm above the surface to mimic the effect of the sun directly on the soil surface during the drying phases. Only the surface of the lysimeter was directly exposed to light, while the lateral walls were covered by a black plastic bag to prevent autotrophic activity inside the system. The bottom of the tank was connected to an external water reservoir to fix the water table level.

2.3. Experimental protocol and Data collection

The infiltration experiment lasted 85 days. By changing the top boundary condition, the lysimeter was subjected to five wetting (W) cycles alternating with five drying (D) cycles of variable duration (see Table 2). The cycles can be classified according to their duration as: medium (W1-D1, W2-D2), long (W3-D3, W5), and short (W4-D4, D5). In the middle of the longest wetting cycle, W3, infiltration was discontinued for a short time, followed by scraping of the top (about 5 cm) before wetting was resumed. This is shown as two distinct cycles in Table 2: W3a, W3b.

Three types of sensors were placed: 5 capacitance sensors (5TE, Decagon Devices) to measure volumetric water content and temperature at depths 5, 15, 30, 45 and 58 (all depths are reported in cm measured from the topsoil); 5 tensiometers (three T5, UMS; and two MPS-2, Decagon Devices) to measure soil water potential also at depths 5, 15, 30, 45 and 58; 2 pressure transducers (Mini-Diver, Schlumberger) to monitor the water table placed at the top and bottom; a third pressure transducer (Baro-Diver, Schlumberger) to record atmospheric variations; and several non-invasive optical sensors (PreSens) to measure partial pressures of oxygen and carbon dioxide (both dissolved and in gas phase). O_2 sensors were placed at depths 5, 15 (2 sensors), 30 (2), 45, 58 (2), plus inlet and outlet, while CO_2 sensors were located at depths 15, 45, inlet and outlet. Measurements of gas phase sensors were corrected to compensate for temperature effects. Figure 1 shows the location of the different sensors.

3. Results: Temporal evolution of infiltration Rates

In each wetting cycle, a quasi-exponential reduction in the infiltration rate with time was observed except for a brief period at the beginning of the experiment, when the system had to adapt to the sudden change in the hydraulic conditions. The time evolution of infiltration rates is presented in Figure 2. During W1 the infiltration rate slightly increased from 200 to 240 L/day. In the remaining wetting cycles, a general trend was observed starting from an initial high value just after the beginning of the cycle, which then decreased rapidly. For example, by the end of W2 the infiltration rate was down to 100 L/day, and was as low as 12 L/day by the end of W5. W4 was too short to observe a decrease in the infiltration rate. At the beginning of all wetting phases the infiltration rate was larger than 200 L/day, indicating a brief period of recovery of the system at the end of each drying period. After scraping in W3, the infiltration rate suddenly recovered, rising from 40 to 200 L/day before decreasing again.

During wetting conditions the water content in the soil approached the porosity values, indicating a high saturation condition. During drying, the water content fell to values, ranging between 0.1 and 0.2, which resulted in capillary pressures that did not exceed 0.2 MPa.

4. Results: Oxygen dynamics

O_2 concentrations displayed distinctive trends both in depth and time associated with the different drying and wetting cycles (Figure 3). Concentrations measured at the pond were always below saturated conditions in equilibrium with the atmosphere, yet higher than those recorded at any sensor within the lysimeter. Oxygen depletion at ponds associated with biological activity has been reported elsewhere (Greskowiak et al., 2005).

4.1. Wetting cycles

During W1, O_2 concentration in the ponding area remained consistent between 8 to 9 mg/L (Figures 3, 4). In the soil, however, during the first 24 h of infiltration, redox conditions underwent a drastic shift. After a transient period when oxygen concentration decreased at all depths, a well-stratified profile of decreasing oxygen with depth was established (Figure 4). Subsequently, O_2 concentration at each depth remained consistent with time.

A similar trend of O_2 concentration was observed at the beginning of W2 with respect to W1, the only difference being the faster depletion of O_2 at depths below 5 cm. O_2 concentrations were consistently low except on day 14 (one day after the start of W2) when a spike of O_2 was observed at all depths, albeit more pronounced near the surface. After day 14, O_2 levels decreased at all depths making the system almost completely anoxic by day 15. Oxygen concentrations in the pond and soil during W3 were consistent with those in W2 except for a faster depletion in the former. Even though a small spike of O_2 was observed a day after the start of W3, the soil remained mainly anoxic for the first four days. A longer spike appeared on day 31 (Figure 3). During scraping (day 34), oxygen levels recovered at all depths. Thereafter, O_2

concentration decreased in an approximately exponential rate but at a slower rate than those observed in the previous wetting phases. Despite W4 follows a long drying period, D3, this wetting cycle showed a dynamic behavior similar to W1 in terms of O_2 distribution. Finally, in W5 O_2 concentration decreased rapidly at all cross-sectional depths, showing a behavior similar to W2 and W3. An unexpected oxygen pulse entered the system on day 78.

4.2. Drying cycles

Figure 5 shows the time evolution of the oxygen in the pond at different depths for the first 5 days after the start of the drying cycles. The partial pressure of O_2 in the ponded water was fairly consistent at 200 hPa for all cycles. The distribution of O_2 along the vertical cross-section lysimeter did not vary much between the 5 drying cycles, displaying very similar distribution patterns. During the first hours of each drying period, oxygen concentrations at all depths recovered rapidly approaching a vertical profile with a clear stratification. Re-oxygenation was slower at greater depths, but eventually oxygen partial pressure reached atmospheric levels at all depths. However, at steady state conditions, partial pressure of soil O_2 remained just below 200 hPa.

5. Interpretation of results and discussion

5.1. Effects of wetting, drying and removal of surface layer on water infiltration dynamics

The infiltration capacity of the system, although roughly constant, increased slightly during W1. This effect may be related to the physical rearrangement of the grain particles at the micro-scale at the start of wetting. Since the soil was hand-packed, the initial water flow rearranged particle locations, generating a new pore distribution and some small scale preferential pathways that changed the overall hydraulic conductivity during the first few days.

After W1, the time evolution of measured infiltration rates during wetting cycles displayed an approximate exponential decrease, down to 60% after W2 and 85% after W3 with respect to the original values at the start of each corresponding cycle. Similar exponential-like decreases in infiltration rates have been reported elsewhere, and are attributed to the decline in permeability because of clogging (e.g., Bouwer, 1978; Pedretti et al., 2012). One result of clogging is a significant decrease in pressure heads in the vertical cross-section below the soil surface where the maximum microbial colonies form (Bouwer, 2002). Of significance is the rate of oxygen depletion during wetting (in absolute value) in W1 with respect to other cycles.

These observations could be attributed to the presence of EPS (extracellular polymeric substances), which are capable of reducing hydraulic conductivity, thus causing clogging (Vandevivere and Baveye, 1992; Thullner et al.,2002). Although not measured in this test, the presence of EPS was observed in the infiltration experiment performed by Rubol et al. (2014) with soil from the same site. Rubol et al. (2014) reported that the soil infiltration capacity decreased during continuous infiltration with significant increase in the water holding capacity at greater depths, where the presence of EPS was more marked. During W1, microbial colonies probably develop (this being quite a relatively slow process). After W2, colonies did not necessarily grow anymore, but EPS were excreted with time, leading to clogging. During the drying phases, the infiltration capacity in the lysimeter reverted to its original value, as EPS reduced its volume. However, the living microbial cells remained active protected from desiccation by EPS (Or et al., 2007).

When the system was re-wetted, a fast recovery of the biological activity was observed in the oxygen profile (Figure 4). A plausible explanation for this occurrence is that the bacterial colonies, still active despite the low water content, had to reactivate or readapt themselves to the increase in water availability under very favorable conditions (presence of water and nutrients).

The infiltration capacity of the system increased following the scraping of the top surface layer (in W3), but it did not reach the value recorded at the start of W3, probably because scraping only affected the top surface whereas clogging occurred at all depths. The subsequent decrease in the infiltration rate with time was again exponential but at a slower rate than at the start of W3. This means that scraping had effectively disturbed the first centimeters of the soil and that the impact of clogging upon permeability continued to be felt. These results are in agreement with those of Mousavi and Rezai (1999), who evaluated the effect of scraping in three artificial recharge basins and found that the treatment was only partially efficient, i.e. restoration of only 68% of the initial infiltration rate. Note, however, that at the start of W4, the infiltration capacity increased again to a high value, suggesting that desiccation is more effective than scraping in terms of infiltration rate recovery.

5.2. O_2 concentration dynamics and changes in biological activity during wetting and drying

Dynamics of O_2 concentrations within the lysimeter during wetting and drying cycles can be attributed to three main processes: flow advection, diffusion in the air phase and O_2 consumption. Once the infiltration front reaches the sensor by advection after the start of a wetting cycle, oxygen concentrations rapidly decline with time owing to biological activity. This is corroborated by the soil CO_2 respiration activity (Figure 7). Figure 6 shows that depletion of oxygen is modeled as a negative exponential function with a first-order decay parameter (λ), which indicates the velocity of the system needed to achieve anoxic conditions:

$$C_{O_2} / C_{O_2,0} = \exp(-\lambda \frac{t}{t_{adv}}) \tag{1}$$

where, $C_{O_2,0}$ is the oxygen value at the surface boundary (z=0), t is time and t_{adv} is the characteristic time of advection based on the flow velocity. The estimated values of λ ranged between 0.0044 (wetting cycle W3b) and 0.0427 (wetting cycle W3a). Hence, at the start of the third wetting cycle, the rate of oxygen consumption was the highest but the value dropped to a minimum after the scraping.

Drainage marks the start of each drying cycle with the result that the advective flow of gas rapidly occupies the pore spaces previously filled by water. After about 3 h of drying, the system reached quasi steady state oxygen conditions displaying a well-defined vertical gradient. A distribution that is characteristic of a combination of diffusion and decay (biological consumption). Assuming that oxygen in air and residual water are in equilibrium, the partial pressure of oxygen, P_{O_2} is governed by

$$D \frac{\partial^2 P_{O_2}}{\partial z^2} - kP_{O_2} = 0 \tag{2}$$

where, D is the effective diffusion coefficient of O_2 [L^2T^{-1}] and k is the first-order de-oxygenation rate based on consumption due to bacterial activity. Integration of this equation gives an exponentially decaying oxygen profile from the value at the surface $P_{O_2,0}$

$$P_{O_2} = P_{O_2,0} \exp(-\sqrt{k / D}\, z) \tag{3}$$

From (3), a characteristic depth (d) can be defined as

$$d = \sqrt{D/k} \tag{4}$$

An effective diffusion coefficient of oxygen of D = 0.0068 cm^2/s was estimated from the Millington and Quirk (1961) model with a gas content of 0.2 and a diffusion coefficient of oxygen in air of 0.2 cm^2/s. Using a characteristic depth d between 20 and 40 cm (other values could be employed here with slightly different results) in equation (4), the first-order de-oxygenation constant k ranges between 1.5 and 0.36 day^{-1}.These values are surprisingly similar to the first-order decay coefficients λ obtained by analyzing the de-oxygenation rates observed in Figure 4 during wetting cycles. This result indicates that the soil was biologically active both during drying and wetting periods. Roberson and Firestone (1992) and Zhang and Yan (2012) reported that bacterial activity remained consistent during both wetting and drying cycles, suggesting that desiccation does not exert a significant effect on cell activity. It should be pointed out that the overall cell activity probably decreased due to the drop in the availability (amount and diversity) of electron acceptors but the activity remained almost intact owing to the availability of oxygen. Given that EPS formation was observed in another infiltration experiment performed with the same soil type (Rubol et al., 2014), we believe that the microbial activity was probably protected by the presence of EPS during drying cycles.

The dynamics between O_2 consumption, biological activity and advection are responsible for a slower reduction of oxygen concentrations during wetting periods compared with the rise in drying periods. The factors influencing the rate of re-aeration are soil type, soil oxygen demand and vadose zone thickness (Neale et al., 2000; Rubol et al., 2013). The high sand percentage in the lysimeter (>99%) was probably instrumental in the high oxygen concentration values reported (Fetter, 1990).

5.3. Relevance of the frequency of monitoring O_2 dynamics

In order to illustrate the effect of oxygen sampling on bio-growth estimates, we employed Monod kinetics to model the rate of growth of biomass using substrate O_2 as the limiting factor. The governing equation is written as

$$\frac{dX}{dt} = \mu_{\max}\left(\frac{C_{O_2}}{K_{O_2} + C_{O_2}}\right)X - K_d X \qquad (5)$$

Where X is the cell biomass concentration, $\mu_{\max}$ is the kinetic coefficient for the maximum specific growth rate, C_{O_2} is the dissolved oxygen concentration, K_{O_2} is Monod's half-saturation constant for dissolved oxygen, and K_d is the parameter to account for the endogenous decay of the biomass. All parameters used in the following simulations (reported by Shaler and Klecka, 1986) are displayed in Figure 8.

The accuracy of the model used for prediction of the rate of biodegradation reactions is considerably improved by the high frequency of measurements. Figure 8 (top) illustrates the variability in dissolved oxygen as a function of time. This is depicted in three sampling strategies in a period close to 3.5 days and corresponding to W1. The figure displays the complete data set recorded by one sensor at a very high frequency (one value every 20 seconds) located at the depth of 5 cm, and two more sensors recording at a relatively low frequency (one value every 4.2 h or 1.16 days, respectively). The main trend of decreasing oxygen concentration with time is observed in all the curves but strong local fluctuations are not shown in the coarser sampling protocols.

Figure 8 (middle) shows the importance of the sampling strategy in terms of the sensitivity of biomass concentration derived from (5) as a function of sampling strategy. Because of the chosen values of the modeling parameters during rewetting cell biomass undergoes little change regardless of our ability to properly characterize oxygen concentrations. The main reason for this is that $C_{O_2} > K_{O_2}$, the latter being equal to 1.2 mg/L. As a consequence, the solution of (5) is very close to an exponential curve, where the increase is caused by $\mu > K_d$.

By day 2.5 there is a sudden increase in oxygen concentration. This is not properly captured by the coarser sampling strategy (see red line in Figure 8, top). Since by that time, the oxygen concentration values are in the order of the value of K_{O_2}, the non-linear limiting effect of C_{O_2} in (5) plays an important role.

Figure 8 (bottom) shows a similar analysis of biomass growth based on the location and the number of sensors used to map the oxygen concentration in the lysimeter. The variability in bacterial concentration is related to the strong non-linearity in (5). As a result, there is a greater sensitivity in the evaluation of bacterial growth and activity as a function of the O_2 concentration sampling resolution. Studies conducted at field scale are only able to record spatiotemporally averaged changes, obscuring the actual dynamics. For example, Kohfahl et al. (2009) modeled oxygen flux rates in groundwater during induced bank infiltration using data obtained from a sampling campaign of 20 measurements in 20 months presented in Massmann et al. (2008). The biogeochemical transport model of the fate of pharmaceutical components during artificial recharge presented by Greskowiak et al. (2006) employed monthly data. Although our study was performed in a laboratory set up and not in the field, we stress the need for a fine (in space and time) sample strategy in order to link the spatial and temporal dynamics of infiltration and O_2 dynamics as a function of depth.

6. Conclusions

This study presents the results of an experiment performed at meso-scale for monitoring infiltration rates and oxygen dynamics under an alternating sequence of wetting and drying conditions, and as a function of depth. Several conclusions may be drawn from this work:

- Infiltration rates affected by clogging revert to the initial values after a short drying period.

- Rewetting reverts drying effects and clogging recovers. Furthermore, after the first wetting period, the rate at which clogging reoccurs is faster than in the first wetting period.

- Scraping reduces clogging and the overall infiltration rate is recovered, but the effects are less pronounced than those of drying. The recovery of the infiltration rate is more effectively achieved by means of desiccation than by scraping the top soil layers.

- The alternation of short wetting and drying cycles does not have a substantial effect on microbial activity, probably because of the protective effects of the EPS surrounding the microbes.

- Oxygen stratification with depth during drying periods is due to a combination of vertical diffusion and O_2 consumption.

- The high variability of oxygen concentrations in space and time necessitates a high sampling frequency if O_2 dynamics affecting different processes are to be considered.

However, it must be ascertained whether the long drying periods offer the same benefits as short drying periods and whether our results transfer to the spatial and temporal distribution of oxygen in Managed Aquifer Recharge or induced recharge facilities.

Acknowledgements

Financial support was provided by the Ministerio de Econonía y Competitividad of the Spanish Government, projects SCARCE (CSD2009-00065) and FEAR (CGL2012-38120). This project received additional funding from the European Union's Seventh Framework Programme for research, technological development and demonstration under grant agreement no PCOFUND-GA-2008-226070. SR acknowledges the support of the Provincia Autonoma di Trento and the European Commission. We also thank Scientific and Technological centers of Universitat de Barcelona for the X-ray diffraction analysis.

References

Akhavan, M., Imhoff, P.T., Andres, A.S., Finsterle, S., 2013. Model evaluation of denitrification under rapid infiltration basin systems. J. Contam. Hydrol. 152, 18-34.

ASTM., 2000. Standard practice for classification of soils for engineering purposes (Unified Soil Classification System). ASTM standard D2487.2000 Annual Book of ASTM Standards.American Society for Testing and Materials (ASTM), Philadelphia, Pa.

Baveye, P., Vandevivere, P., Hoyle, BL., DeLeo, PC., Sanchez de Lozada, D., 1998. Environmental impact and mechanisms of the biological clogging of saturated soils and aquifer materials. Crit. Rev. Environ. Sci. Technol. 28(2), 123-191.

Bouwer, E.J., 1994. Bioremediation of chlorinated solvents using alternate electron acceptors. Handbook of Bioremediation, Boca Raton, Florida: Lewis, pp 149-175.

Bouwer, H., 1978. Groundwater Hydrology. McGraw-Hill Book Company, New York.

Bouwer, H., Rice, R.C., 1984. Renovation of wastewater at the 23rd Avenue rapid infiltration project. Water Pollut. Control Federation. 76-83.

Bouwer, H., Rice, R.C., 2001. Capturing flood waters for artificial recharge of groundwater. Proc 10th Biennial Symp Artificial Recharge of Groundwater.Hydrol. Soc. 99-106

Bouwer, H., 2002. Artificial recharge of groundwater: hydrogeology and engineering. Hydrogeol. J. 10(1), 121-142.

Christensen, T.H., Bjerg, P.L.,Banwart, S.A., Jakobsen, R., Heron, G., Albrechtsen,H.J., 2000. Characteristics of redox conditions in groundwater contaminant. J. Contam. Hydrol. 45(3-4), 165-241.

Constantz, J., 1982. Temperature dependence of unsaturated hydraulic conductivity of two soils.Soil Sci. Soc. Am. J. 46(3), 466-470.

DeAngelis, K.M., Silver, W.L., Thompson, A.W., Firestone, M.K., 2010. Microbial communities acclimate to recurring changes in soil redox potential status. Environ. Microbiol. 12(2), 3137-3149.

Dillon, P., 2005. Future management of aquifer recharge.Hydrogeol.J. 13(1), 313-316.

Dutta, T., S, Rubol., 2014. Effect of spatial heterogeneity on rate of sedimentary O_2 consumption reaction. In: E. Pardo-Igúzquiza et al. (eds.), Mathematics of Planet Earth, Lecture Notes in Earth System Sciences, Berlin Heidelberg, pp 485-489.

EPA US, 1984. Process design manual for land treatment of municipal wastewater, supplement on rapid infiltration and overland Flow. (EPA 625/1-81-013a).

Fernandez-Turiel, J.L., Gimeno, D., Rodriguez, J.J., Carnicero, M., Valero, F., 2003. Spatial and seasonal variations of water quality in a Mediterranean catchment: the Llobregat River (NE Spain). Environ. Geochem. Health 25(4), 453-474.

Fetter, C.W., 1990. Applied Hydrogeology, second ed. Columbus: Merrill Pub. Co.

Fox, P., Houston, A.R., Westerhoff, P., 2006. Advances in soil aquifer treatment research for sustainable water reuse. AWWA Research Foundation.

Greskowiak, J., Prommer, H., Massmann, G., Johnston, C.D.,Nutzmann, G., Pekdeger, A., 2005. The impact of variably saturated conditions on hydrogeochemical changes during artificial recharge of groundwater. Appl. Geochem. 20, 1409-1426.

Greskowiak, J., Prommer, H., Massmann, G., Nutzmann, G., 2006. Modeling seasonal redox dynamic and the corresponding fate of the pharmaceutical residue phenazone during artificial recharge of groundwater. Environ. Sci. Technol. 40(21), 6615-6621.

Jaynes, D.B., 1990. Temperature Variations Effect on Field-Measured Infiltration. Soil Science Soc. Am. J. 54(2), 305-311.

Kohfahl, C., Massmann, G., Pekdeger, A., 2009. Sources of oxygen flux in groundwater during induced bank filtration at a site in Berlin, Germany. Hydrogeol. J. 17(3), 571-578.

Krause, S., Boano, F., Cuthbert, M.O., Fleckenstein, J.H., Lewandowski, J., 2014. Understanding process dynamics at aquifer-surface water interfaces: An introduction to the special section on new modeling approaches and novel experimental technologies. Water Resour. Res. 50(2), 1847-1855.

Le Bihan, Y., Lessard, P., 2000. Monitoring biofilter clogging: biogeochemical characteristics of the biomass. Water Res. 34(17), 4284-4294.

Massmann, G., Nogeitzig, A., Taute, T., Pekdeger, A., 2008. Seasonal and spatial distribution of redox zones during lake bank filtration in Berlin, Germany. Environ. Geology 54(1), 53-65.

McCarty, L., Semprini, P.L., 1994. Ground-water treatment for chlorinated solvents. Handbook of Bioremediation, Boca Raton, Florida: Lewis, pp 87-116.

McClain, M.E., Boyer, E.W., Dent, C.L., Gergel, S.E., Grimm, N.B., Groffman, P.M., Hart, S.C., Harvey, J.W., Johnston, C.A., Mayorga, E., McDowell, W.H., Pinay, G., 2003. Biogeochemical hot spots and hot moments at the interface of terrestrial and aquatic ecosystems.Ecosyst. 6(4), 301-312.

Millington, R.J., Quirk, J., 1961. Permeability of porous solids.Trans. Faraday Soc. 57, 1200-1207.

Mousavi, S.F., Rezai, V., 1999. Evaluation of scraping treatments to restore initial infiltration capacity of three artificial recharge projects in central Iran. Hydrogeol. J. 7(5), 490-500.

Neale, C., Hughes, J.B., Ward, C.H., 2000. Impacts of unsaturated zone properties on oxygen transport and aquifer rearetaion. Ground Water 38(5), 784-794.

NRMRI, 2006.Process design manual; Land treatment of municipal wastewater effluents.

Or, D., Phutane, S., Deschene, A., 2007. Extracellular polymeric substances affecting pore-scale hydrologic conditions for bacterial activity in unsaturated soils.Vadose Zone J. 6, 298–305.

Pedretti, D., Barahona-Palomo, M., Bolster, D., Fernàndez-Garcia, D., Sanchez-Vila, X., Tartakovsky, D.M., 2012. Probabilistic analysis of maintenance and operation of artificial recharge ponds. Advances Water Resour. 36, 23–35.

Rifai, H.S., Borden, R.C., Wilson, J.T., Ward, C.H., 1995. Intrinsic bioattenuation for subsurface restoration. Intrinsic bioremediation 1-29.

Roberson, E.B., Firestone, M.K., 1992. Relationship between dessication and exopolysaccharide production in a soil Pseudomonas sp. Appl. Environ.Microbiol.58(4), 1284–1291.

Romaní, A.M., Guasch, H., Muñoz, I., Ruana, J., Vilalta, E., Schwartz, T., Emtiazi, F., Sabater, S., 2004. Biofilm structure and function and possible implications for riverine DOC dynamics.Microb. Ecol. 47(4), 316-328.

Rubol, S., Silver, W.L., Bellin, A., 2012. Hydrologic control on redox and nitrogen dynamics in a peatland soil. Sci. Total Environ. 432, 37-46.

Rubol, S., Manzoni, S., Bellin, A., & Porporato, A., 2013. Modeling soil moisture and oxygen effects on soil biogeochemical cycles including dissimilatory nitrate reduction to ammonium (DNRA). *Advances in Water Resources*, *62*, 106-124.

Rubol,S., Freixa, A., Carles-Brangarí, A., Fernàndez-Garcia, D., Romaní, A.M., Sanchez-Vila, X., 2014. Connecting bacterial colonization to physical and biochemical changes in a sand box infiltration experiment. Hydrogeolog. J. 517, 217-327.

Schimel, J., Balser, T.C., Wallenstein, M., 2007. Microbial stress-response physiology and its implications for ecosystem function.Ecol. 88(6), 1386-1394.

Schmidt, C.M., Fisher, A.T., Racz, A.J., Lockwood, B.S., Huertos, M.L., 2011. Linking denitrification and infiltration rates during managed artificial recharge. Environ. Sci. Technol. 45(22), 9634-9640.

Shaler, T.A., Klecka, G.M., 1986. Effects of dissolved oxygen concentration on biodegradation of 2,4-dichlorophenoxyacetic acid. Appl. Environ. Microbiol. 51, 950–955.

Thullner, M., Zeyer, J., Kinzelbach, W. 2002. Influence of microbial growth on hydraulic properties of pore networks. Transport in Porous Media 49, no. 1: 99–122.

Vandevivere, P., and Baveye, P., 1992. Effect of bacterial extracellular polymers on the saturated hydraulic conductivity of sand columns. Appl. Environ. Microbiol. 58(5), 1690-1698.

Vogel, T., 1994. Natural bioremediation of chlorinated solvents. Handbook of Bioremediation*,* Boca Raton, Florida: Lewis, pp 201-225.

Zhang, Q., Yan, T., 2012. Correlation of intracellular Trehalose concentration with desiccation resistance of soil Escherichia coli populations, Appl. Environ.Microbiol. 78 (20), 7407–7413.

Table 1. Composition of the synthetic water used in the infiltration experiment (in mg/L).

Na^+	**K^+**	**Ca^{2+}**	**Mg^{2+}**	**Cl^-**	**$NO3^-$**	**$SO4^{2-}$**	**$HCO3^-$**	**$NH4^+$**	**$PO4^{3-}$**	**$SiO3^{2-}$**	**Cellobiose**	**Leucine-proline**	**Humic acid**
159.3	39.9	120.2	34.0	343.9	12.1	202.7	145.2	1.7	1.0	12.5	1.5	1.5	7.0

Table 2. Information about the duration of the individual cycles in the experiment

Cycle	Abbreviation	Length
First wetting cycle	W1	5d 11h
First drying cycle	D1	7d 13h
Second wetting cycle	W2	6d 6h
Second drying cycle	D2	7d 18h
Third wetting cycle	W3a	7d 12h
	W3b	6d 14h
Third drying cycle	D3	25d 22h
Fourth wetting cycle	W4	2d 8h
Fourth drying cycle	D4	4d 17h
Fifth wetting cycle	W5	10d 23h

Fifth drying cycle	D5	1h

Table 3. Characteristics of the sediments

pH	OC(%)	NH4-N (mg-N/Kg)	NO3-N (mg-N/Kg)	Medium sand(%)	Fine sand(%)	Finer material (%)
7.6	2	2	5	81.8	17.67	0.52

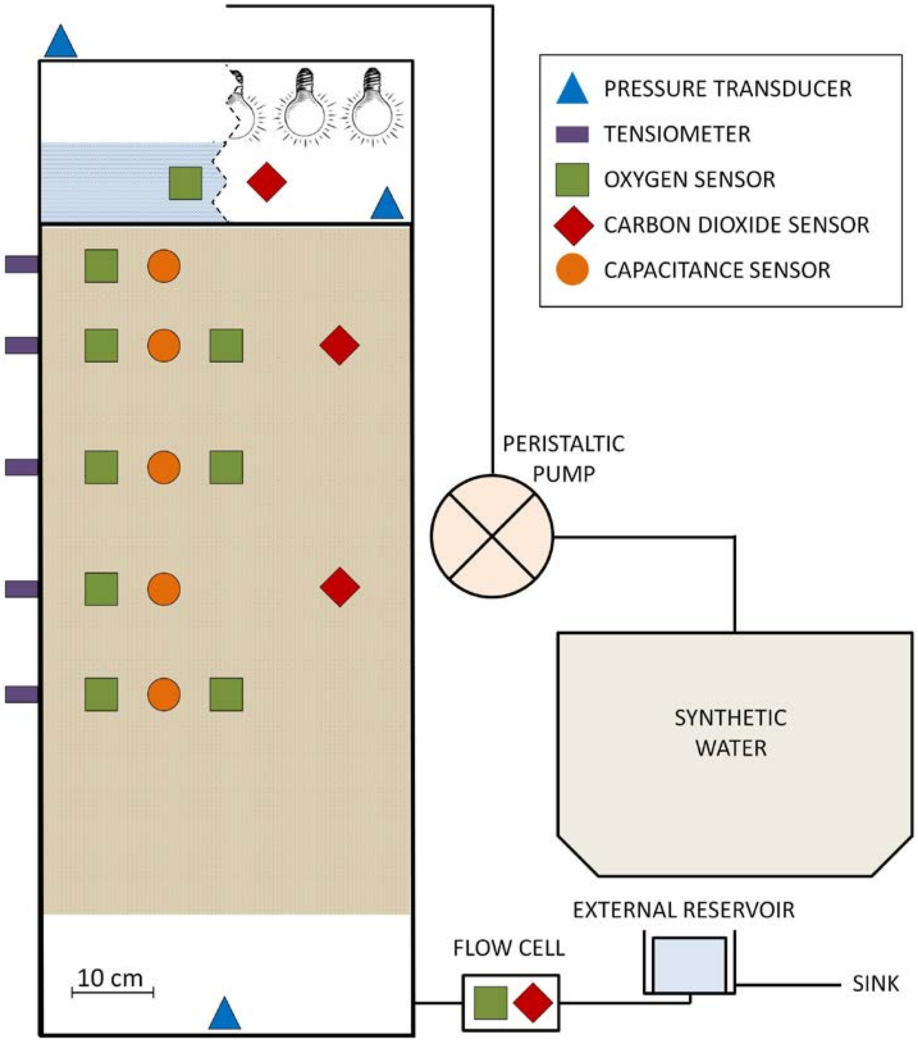

Figure 1. Sketch of the experimental setup showing the body of the lysimeter, the location of the sensors and input/output water systems. The boundary condition active during wetting is a constant ponding (left side of the tank) and light bulbs during drying periods (right side in the ponding area).

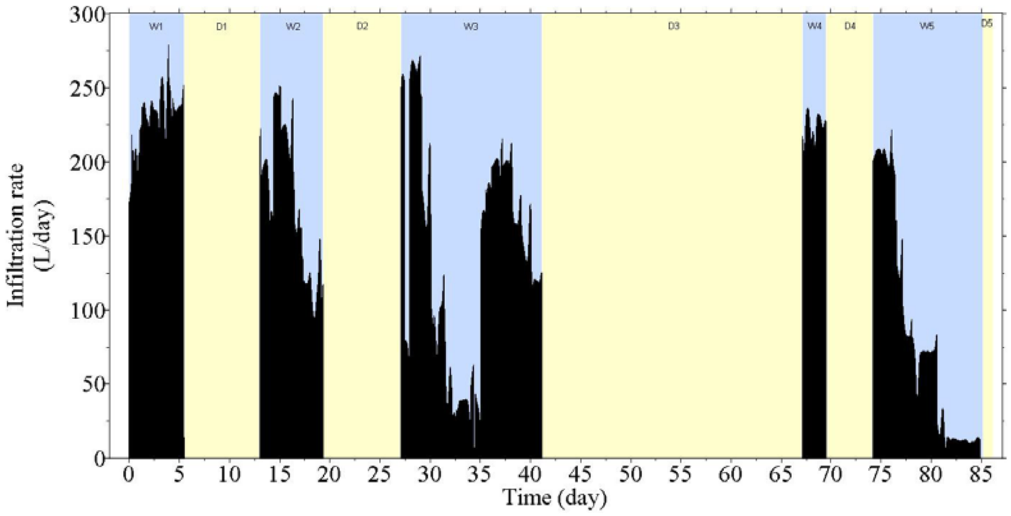

Figure 2. Evolution of the infiltration rate (in L/day) with time during the experiment. Blank areas correspond to drying phases.

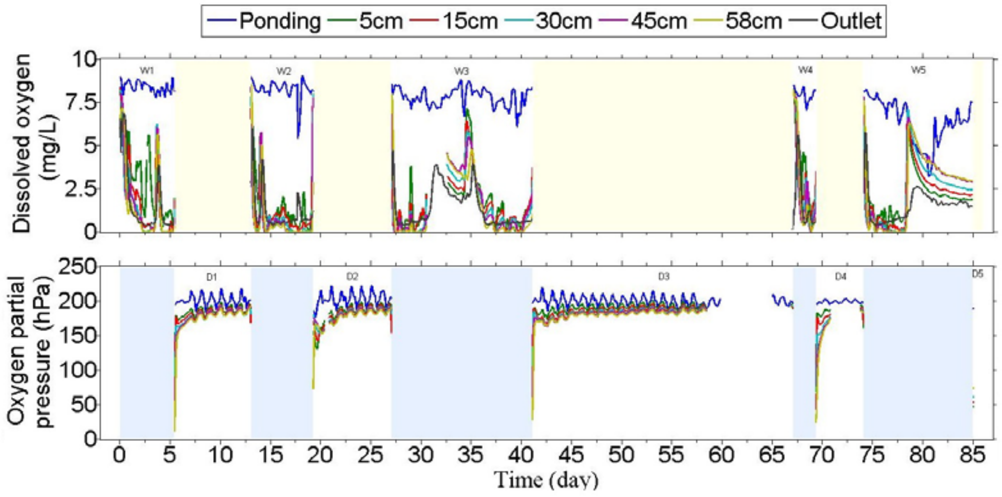

Figure 3. O_2 concentration at the ponding and at different depths of soil across the vertical length of the lysimeter during wetting (measured as dissolved oxygen in mg/L) and drying cycles (measured as oxygen partial pressure in hPa). The values at depths 15, 30 and 58 correspond to

the arithmetic average of the duplicate sensors. The reported sampling variances are ($\sigma^2_{15cm} = 0.015$, $\sigma^2_{30cm} = 0.008$, $\sigma^2_{58cm} = 0.013$).

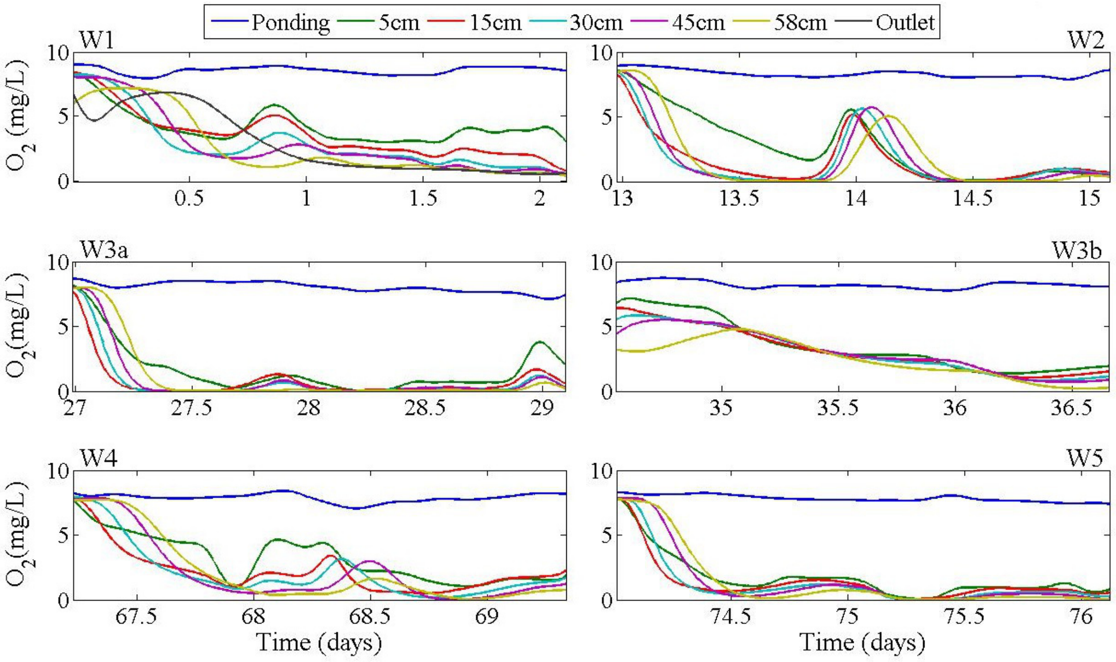

Figure 4.O_2 concentration dynamics at the start of each wetting cycle; plots report the changes during the first two days of each wetting cycle (from W1 to W5). The values at depths 15, 30 and 58 correspond to the arithmetic average of the duplicate sensors. The sampling variances are ($\sigma^2_{15cm} = 0.015$, $\sigma^2_{30cm} = 0.008$, $\sigma^2_{58cm} = 0.013$).

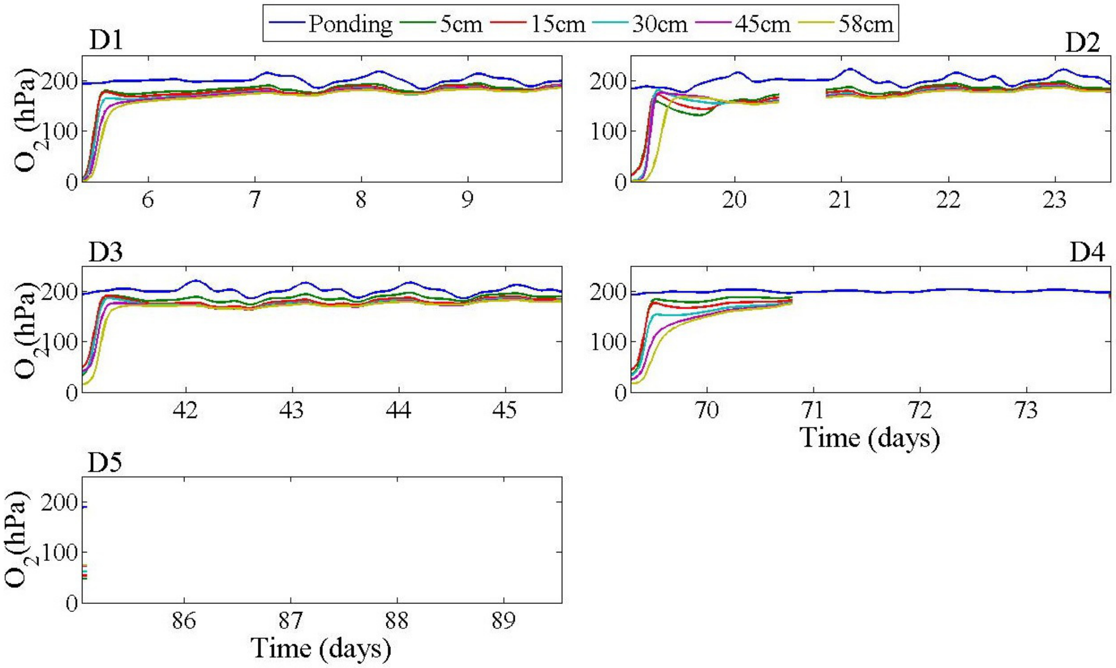

Figure 5. Dynamics of O_2 at the start of each drying cycle for 5 days (D5 lasted only 1h). The values at depths 15, 30 and 58 correspond to the arithmetic average of the duplicate sensors. The sampling variances are ($\sigma^2_{15cm} = 0.015$, $\sigma^2_{30cm} = 0.008$, $\sigma^2_{58cm} = 0.013$).

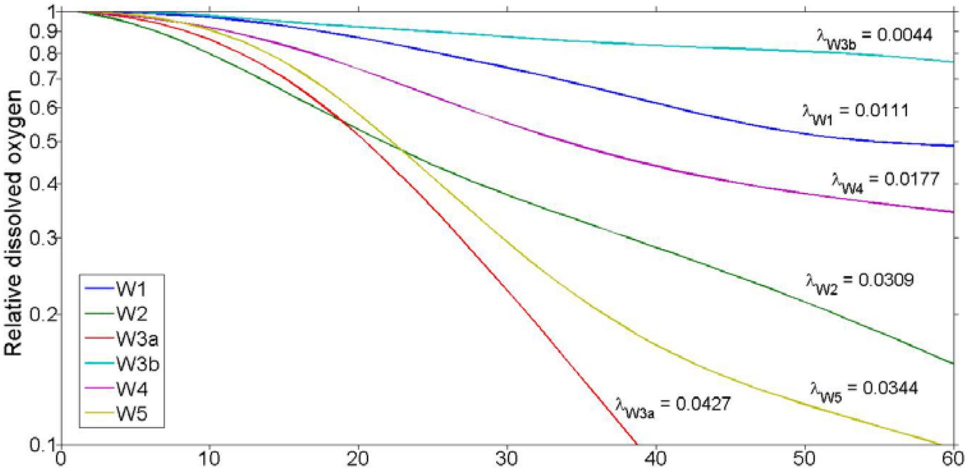

Figure 6. Relative dissolved oxygen concentration at the start of each wetting cycle. Oxygen depletion is a function of both transport and consumption mechanisms. Parameter λ is the decay parameter in a negative exponential function.

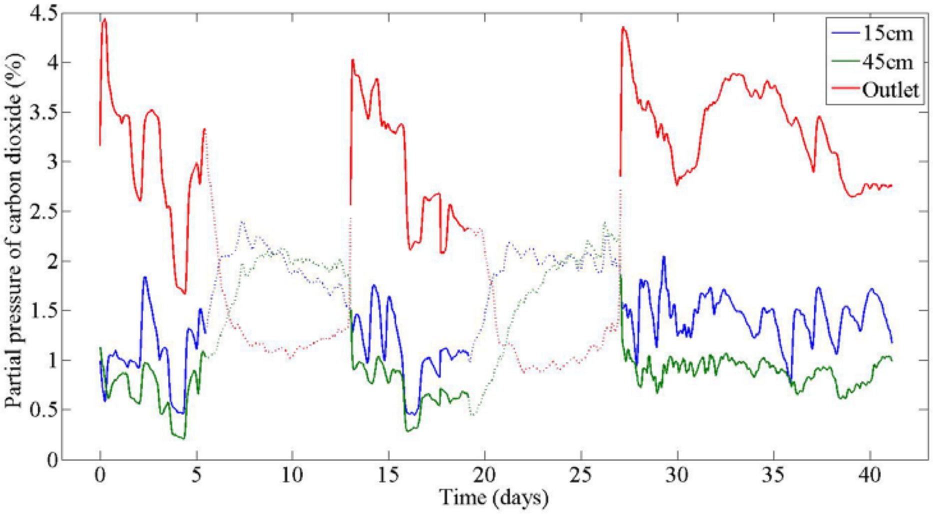

Figure 7. Partial pressure of CO_2 (%pCO_2) during wetting (solid lines) and drying cycles (dotted lines). CO_2 sensor requires 99% humidity for proper functioning, so data during drying cycles are not shown.

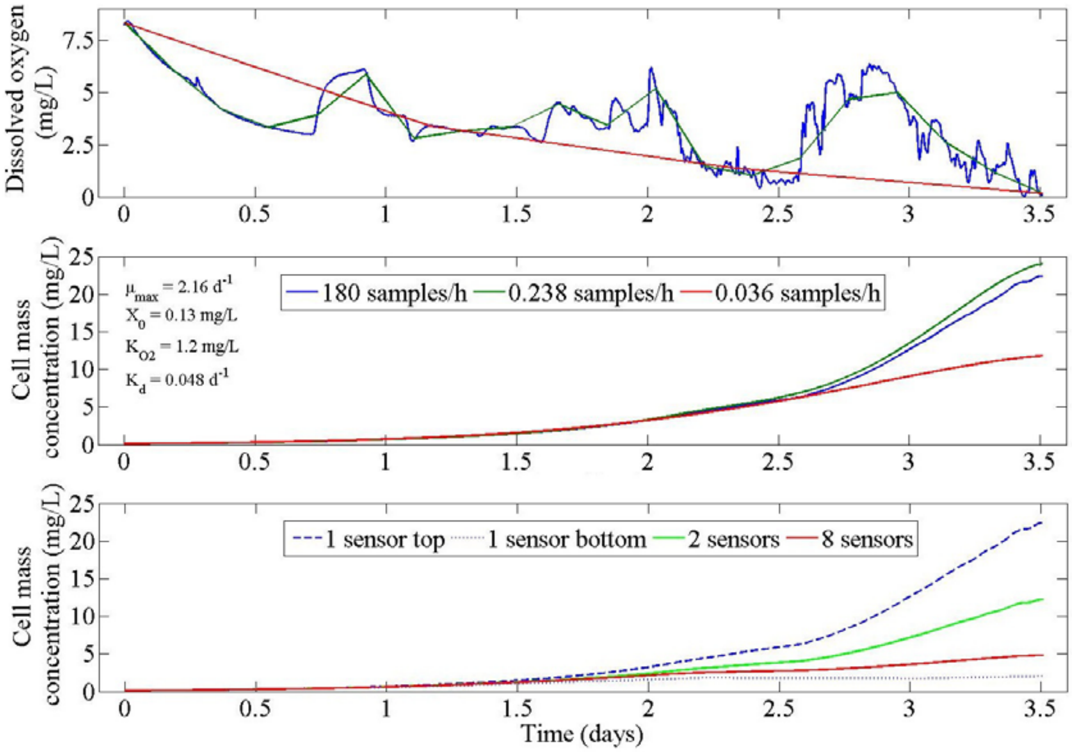

Figure 8. Top: Dissolved oxygen concentration dynamics during the first 3.5 days of W1. Different lines depict measurements from specific monitoring resolution strategies: 180 samples/hour in blue, 0.238 samples/hour in green, and 0.036 samples/hour in red. Middle: Cell biomass concentrations estimated from (5) considering oxygen as the growth-limiting factor corresponding to the three sampling densities. Bottom: Biomass concentration growth deduced from (5) by using the data obtained in individual sensors or in a combination of them.